Renewable Energy 255 (2025) 123765

Contents lists available at ScienceDirect

Renewable Energy

journal homepage: www.elsevier.com/locate/renene

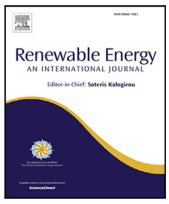

The co-location of wind and wave energy at multiple global sites

Aidan Sewter *, Simon P. Neill

School of Ocean Sciences, Bangor University, LL59 5AB, United Kingdom

ARTICLE INFO

Dataset link: https://cds.climate.copernicus.eu/cdsapp#!/dataset/reanalysis-era5-single-levels?tab=form, https://nrel.github.io/turbine-models/IEA_15MW_240_RWT.html

Keywords:
Hybrid energy systems
Grid stability
Ocean energy
Resource synergy
Global model

ABSTRACT

The variability of wind energy necessitates continued reliance on fossil fuel power sources as baseload, hindering the integration of renewable energy. This study proposes co-locating Wave Energy Converters (WECs) with Offshore Wind Turbines (OWTs) to partly mitigate these issues, adopting a 'topping-up' strategy, integrating WEC capacity into existing OWT arrays. Using the ERA5 global reanalysis dataset, global wind and wave resources, their correlation and various other metrics were calculated. Four regions – Western Australia, Brazil, Pacific coast USA, and Portugal – were chosen for co-location based on their favourable conditions. Applying theoretical resources to four WEC technologies and a 15 MW reference OWT, a sensitivity analysis was conducted across the study sites, considering downtime, normalised power output, and variability. Australia demonstrated enhanced power stability (27.2% less variability) when WECs were applied. Brazil demonstrated significant improvement (26.3% less variability), with USA and Portugal also displaying performance enhancement (21.72% and 16.32%, respectively, less variability). Southern Hemisphere sites benefit from seasonal offset peaks in resource phase, reducing overall variability. Swell-driven wave climates contribute to smoother combined power output due to phase delays between resources. This study serves as a global co-location framework, facilitated by the ERA5 dataset, allowing replication for diverse locations worldwide.

1. Introduction

In recent years, the global transition towards sustainable energy has accelerated due to the growing population and intensifying climate crisis [1,2]. Wind energy, as one of the leading renewable energy resources, has seen significant advancements, particularly offshore, which offers greater energy potential and reduced land use conflicts compared to their onshore counterparts. This development has enhanced the economic competitiveness of offshore wind compared to established sources of electricity generation [3,4]. In 2023, global offshore wind capacity reached 75 GW, marking a 24% increase from 2022, with projections indicating growth to 487 GW by the end of 2033 [5]. However, a major challenge impeding the full integration of wind energy into power grids is its inherent variability. Wind speeds fluctuate over time and space, leading to inconsistent electricity generation that cannot always meet demand; research suggests that electrical networks have shifted towards wind-dominated regimes [6], and numerous other studies cite this inherent variability as an obstacle in providing baseload power by wind and its further penetration into the electricity market [7,8]. To compensate for this intermittency, power grids currently rely on fossil fuel-based baseload generation, which ensures grid stability but contradicts decarbonisation efforts [9]. This dependence on fossil fuels limits the potential for increased Ocean Renewable Energy (ORE) penetration and hinders progress towards climate goals.

The necessity of addressing wind energy variability is further emphasised by geopolitical and economic disruptions in fossil fuel supplies. A notable example occurred in 2022 when Russia significantly reduced gas exports to Europe in response to European support for Ukraine, highlighting the vulnerabilities associated with fossil fuel dependence [10]. A more resilient energy system requires solutions that reduce reliance on conventional baseload power while enhancing renewable energy reliability.

ORE options, such as energy storage [11], tidal stream [12], tidal range [13], and wave power [14], offer a promising avenue for addressing wind energy variability. Among these, wave energy is particularly well-suited as a complementary resource. Unlike wind, wave energy exhibits lower short-term variability and often persists even when wind speeds decline. Wave energy is also significantly less variable over short time scales (hourly) compared to other marine resources, a characteristic that is required to reduce the variability of wind energy conversion. For example, and in contrast, tidal stream is a discontinuous source of energy, only generating power for 6–12 hours per day.[1] The global theoretical wave energy resource is estimated at

* Corresponding author.
E-mail address: asewter@gmail.com (A. Sewter).

[1] It is also noted that tidal energy suffers from variability at the fortnightly – spring-neap – timescale.

https://doi.org/10.1016/j.renene.2025.123765
Received 1 March 2024; Received in revised form 13 May 2025; Accepted 13 June 2025
Available online 28 June 2025

approximately 2 TW, comparable to total global energy demand [14,15]. If effectively harnessed, wave energy could play a strategic role in achieving net-zero emissions by 2050, and help limit global temperature rise below two degrees Celsius compared to pre-industrial levels (1850–1900), as outlined in the Paris Agreement [16,17].

Despite its potential, wave energy faces significant economic barriers, primarily due to its high Levelised Cost of Energy (LCoE) [18,19]. However, co-locating Wave Energy Converters (WECs) with Offshore Wind Turbines (OWTs) presents an economically viable strategy. Since wind and wave resources often occupy the same spatial footprint, as shown by Gao et al. [20] in their assessment of hybrid resource potential in Australia and by Wen et al. [21] in their analysis of joint exploitation feasibility along China's southeast coast, their combined deployment can help mitigate wind energy fluctuations and produce a more stable power output. This is particularly beneficial in regions where wave climates are quasi-independent of the wind climate (regions dominated by swell waves); the two resources will have a weaker correlation and be more effective at reducing power output variability, leading to an overall more consistent (aggregated) power output [22]. Co-location is only attractive in these situations; when the two resources are strongly correlated (local wind-driven wave climates, for example in semi-enclosed seas), the potential to reduce variability is highly restricted [23].

Numerous studies have explored the benefits of co-locating OWTs and WECs. Stoutenburg et al. [24] highlighted how the co-location of OWTs and WECs could reduce power variability and power outages; in California, co-located wind-wave farms were found to have the potential to reduce annual power outages to just 100 h, compared to over 1000 h for standalone wind farms and more than 200 h for wave farms. Similar research in Ireland supports these findings, demonstrating that co-located farms provide significant advantages in suitable climates [25]. Economic assessments indicate that while floating offshore wind energy remains the most cost-effective option, co-located floating wind-wave systems outperform standalone wave farms [26]. Moreover, integrating floating OWTs with WECs is considered a viable hybrid approach that enhances electricity generation while reducing overall costs [27]. Kluger et al. [28] investigated the integration of WECs into offshore wind farms equipped with energy storage. Their findings indicated that a 50:50 wind-wave farm has the potential to reduce farm output variability by 16%, decrease power curtailment by 7%, and increase grid efficiency by 2% compared to a 100% wind farm. This integration not only enhanced supply–demand matching but also improved the overall efficiency and reliability of renewable energy systems.

This study aims to quantify the performance benefits of combining wind and wave energy converters across multiple global sites. Despite significant advancements in offshore wind energy, its variability remains a critical barrier to achieving high levels of renewable energy penetration. While previous research has explored co-locating wind and wave energy, most studies have focused on capacity displacement rather than augmentation. To address this research gap, this study investigates the benefits of a 'topping-up', or augmenting, approach, where WEC devices are added to an OWT array in operation, construction, or planning, rather than displacing OWT capacity. By enhancing existing offshore wind farms with WECs, this approach aims to improve grid stability and economic feasibility. This approach represents the most economically viable option for WEC deployment at present, leveraging existing infrastructure to achieve cost savings. Although a comprehensive analysis of these cost savings is beyond the scope of this study, they have been thoroughly examined by Astariz et al. [18,29]. Additionally, the technological challenges associated with integrating WECs with OWTs, environmental impacts, and the effects of wake interactions between ORE infrastructure are not within the scope of this study. The study aim will be addressed by the following objectives:

(i) Source wind and wave data at appropriate spatial and temporal resolutions using the ERA5 global reanalysis dataset.
(ii) Use the 4C Offshore global renewable database to understand areas currently under development for renewable energy projects. These locations will aid site selection.
(iii) Conduct bulk (spatial and temporal) analysis by calculating the theoretical wind and wave resources. This will show possible regions that exhibit favourable phasing between wind and waves.
(iv) Statistical metrics, such as linear correlation, cross-correlation, and variability will be calculated to quantify and understand the synergy between the resources at various locations.
(v) Investigate selected sites in detail and optimise the joint occurrence using the technical resource. Device power curves for various technology types (including attenuators and point absorbers) will be applied to address this objective.

2. Data & methodology

2.1. Data sources

The European Centre for Medium-Range Weather Forecast (ECMWF) ERA5[2] dataset is used for this study. ERA5 is a fifth generation ECMWF reanalysis of the global climate. It provides estimates on single and multiple levels for a large number of atmospheric, ocean-wave, and land-surface quantities. Atmospheric data is provided at a spatial resolution of 0.25×0.25°, and ocean waves at 0.5×0.5° [30,31], at hourly time-steps, from 1940–present. ERA5 has been extensively validated, for both the purposes of wind and wave power, with metocean values deemed suitable for power analysis [32,33]. ERA5 was selected because of its global nature; data can be accessed for any location on Earth, something that is not possible with deployed instruments or regional models[3] [23]. This methodology is therefore easily relocatable to any region of interest. Global values for significant wave height H_s, mean wave period T_m, peak wave period T_p, and the 10 m components of eastward and northward wind were accessed. During the initial global analysis, data spanning 2020 was selected for analysis, for 2928 three-hourly data points at each grid point. Once specific study sites were identified for further analysis, data was selected spanning 11 years (2012–2022), resulting in 96,432 hourly data points at each location (i.e. three-hourly data was used for the initial bulk analysis, followed by one hourly data for the detailed analysis). This data period was selected to prioritise a balance between computational feasibility and what was most relevant to recent climatic conditions, all while maintaining adequate data volume and capturing necessary interannual fluctuations.

Within the ECMWF ocean model output parameters [34], H_s is defined as $H_s = 4\sqrt{m_0}$, where m_0 is the 0th moment of spectral density. T_m is based on the moment of order -1: $T_m = T_{m-10} = m_{-1}/m_0$. T_m is more commonly referred to as mean wave energy period (T_e), therefore ERA5 T_m will be referred to as T_e hereafter.

2.2. Raw data analysis methodology

2.2.1. Wind power

The ERA5 dataset provides wind data as the 10 m u-component of wind (u) and 10 m v-component of wind (v). Initially, wind speed (U) is calculated using:

$$U = \sqrt{u^2 + v^2} \tag{1}$$

For the application of wind speed to OWTs, wind speed needs to be calculated at hub height. The power law wind profile is applied [35]:

$$U = U_r \left(\frac{Z}{Z_r} \right)^{\alpha} \tag{2}$$

[2] ERA5 refers to ECMWF Reanalysis v5
[3] While ERA5 was selected for this study, similar global coverage can also be achieved using other global reanalysis models

where U and U_r are wind speed at hub height Z and reference height Z_r. α is the shear exponent, applied as 0.11 in this study as neutral atmospheric stability is assumed. This is a reasonable assumption over the open ocean, and has been used extensively in the literature [35,36].

The theoretical wind resource was estimated by calculating Wind Power Density (WPD) in units of W/m^2:

$$WPD = \frac{1}{2}\rho_a U^3 \tag{3}$$

where ρ_a is air density, 1.225 kg m^{-3} in this study.

2.2.2. Wave power

The theoretical wave resource was estimated by calculating Wave Power Flux (WPF) per metre of wave crest (W/m). Considering deep water conditions, H_s and T_e can be used directly to give a measure of WPF:

$$WPF = \frac{\rho_w g^2}{64\pi} {H_s}^2 T_e \tag{4}$$

where g is gravitational acceleration (9.81 m/s^2), H_s is significant wave height, ρ_w is the density of seawater (1023 kg/m^3), and T_e is wave energy period. Deep water conditions were selected for this study, as water depth exceeds the wavelength for all locations selected. Deep water assumptions also ease global analysis, as one equation can be applied to all spatial and temporal positions.

2.3. Statistical metrics

Less variable power output will only occur if the wind and wave resources are out of phase with one another. Pearson's linear correlation is a metric that can be used to quantify this, as used by Wen et al. [21] and Kalogeri et al. [37] within the context of joint wind/wave analysis. It is calculated using:

$$R = \frac{1}{N}\sum_{i=1}^{N} \frac{(P_{wind,i} - \overline{P}_{wind})(P_{wave,i} - \overline{P}_{wave})}{\sigma P_{wind}\ \sigma P_{wave}} \tag{5}$$

where $P_{wind,i}$, $P_{wave,i}$ represent instantaneous WPD and WPF, respectively, at index i. $\overline{P}_{wind}$ and $\overline{P}_{wave}$ represent the mean values of WPD and WPF, respectively, while σP_{wind} and σP_{wave} represent their respective standard deviations. Lower values represent more favourable conditions, as the two resources peak at different times. The cross-correlation coefficient is another metric used to find similarities or patterns between two time-series datasets and identify time shifts (lag) between them. It is calculated using [25]:

$$c(\tau) = \frac{1}{N}\sum_{k=1}^{N-\tau} \frac{[P_{\text{wind}}(k) - \mu_{\text{wind}}][P_{\text{wave}}(k+\tau) - \mu_{\text{wave}}]}{\sigma_{\text{wind}}\sigma_{\text{wave}}} \tag{6}$$

where μ_{wind}, μ_{wave}, and σ_{wind}, σ_{wave} are the mean and the standard deviation of P_{wind} and P_{wave}, respectively. $c(\tau)$ represents the correlation at time lag, τ. To gauge the overall stability of the combined output the Coefficient of Variability (CoV) can be calculated using [21]:

$$CoV = \frac{\sigma P_t}{\overline{P_t}} \tag{7}$$

where σP_t is the standard deviation of the aggregated (combined) output, normalised by the mean of the aggregated output, $\overline{P_t}$. CoV is a measure of how widely spread values are around the mean, normalised by the mean output. This produces a dimensionless measure which can be compared to other locations and scaled regardless of the absolute power of any particular array. Values will vary between 0 and 1, with lower values representative of a less variable power output.

Another useful metric is Wind and Wave Synergy (WIWAS) [21]:

$$WIWAS = \frac{\text{No. of hours}(P_{\text{wind}} > 80\,\text{W/m}^2 \text{ or } P_{\text{wave}} > 2.5\,\text{kW/m})}{\text{Total no. of hours}} \tag{8}$$

Table 1
Information regarding the reference 15 MW OWT used in this study [39].

OWT	IEA 15MW
Nominal Power (MW)	15
Cut-in Wind Speed (m/s)	3
Cut-out Wind Speed (m/s)	25
Hub Height (m)	150

The threshold WPD was set to 80 W/m^2 as this is the power density when the cut in speed of a 15 MW OWT[4] is met (>3 m/s) [38,39]. Similarly, 2.5 kW/m was selected for the threshold WPF as it corresponds with the typical cut in significant wave height and energy period of WECs (>1 m and >5 s, respectively) [21,40]. The threshold values have been altered from the original equation by Wen et al. [21] to represent the performance of the WECs and OWTs considered in this study.

To aid the site selection process, a new metric was developed which combines the results produced by WIWAS and linear correlation; Wind Wave Correlation Synergy (WWCS). It is calculated using:

$$WWCS = \frac{(1-R)/(1-R_{\text{min}}) + WIWAS/WIWAS_{\text{max}}}{2} \tag{9}$$

R_{min} and $WIWAS_{max}$ represent the minimum and maximum for R (Eq. (5)) and WIWAS (Eq. (8)), respectively. Output values will vary between 0 and 1, with larger values representative of locations more suitable for co-location.

2.4. Site selection

Initially, values for the theoretical wind and wave energy resource, WIWAS (Eq. (8)), linear correlation (Eq. (5)) and WWCS (Eq. (9)) were calculated on a global grid for a single, arbitrary, year — 2020. These values were then plotted to locate potential sites that would be suitable for a co-located energy conversion system. This selection process was combined with the 4C Offshore wind database [41] to establish which regions have OWT arrays in operation, construction or in planning. Once these criteria have been satisfied, four study sites across the globe were selected for further analysis: Mid-West array in Western Australia, Ventos Fluminenses in Southeastern Brazil, Olympic Wind in Northwestern (Pacific coast) USA, and Botafogo in Midwestern Portugal. These sites were selected based on their energetic wind and wave resources, favourable resource phase-lag, WWCS, and OWT array status. Further details about these sites are included in Section 3.1 and Section 3.2.1.

2.5. Selection of OWT and WEC devices

To quantify the technical application of combined systems, the estimated theoretical resources will be applied to various device power curves and power matrices. The selection of the OWT power curve will depend upon the capacity of the selected OWT array. As the specific power curves for devices are highly protected intellectual property of the manufacturers, the International Energy Agency (IEA) reference 15 MW turbine will be used. Details about the reference device can be found in Table 1, with the specific power curve in Fig. A.1.

Considering WECs, these devices are in their infancy compared to OWTs. A variety of devices will therefore be applied to each site to aid the understanding of the performance of each device in different wave climates. Details about the WEC devices used in this study can be found in Table 2, with the specific power matrices in Figs. A.2, A.3, A.4. Pelamis, SeaPower, and Archimedes WaveSwing (AWS) were selected as they represent well-researched, and ocean tested, technologies with

[4] When considering the reference International Energy Agency (IEA) 15 MW OWT used in this study (see Table 1).

Table 2
Information regarding WECs used in this study.

WEC	Nominal Power (MW)	Classification	Power Matrix Resolution (m ×s)	Source
Pelamis	0.76	Attenuator	0.5 × 0.5 ($Hs \times Te$)	[43]
SeaPower	3.587	Attenuator	0.5 × 1.0 ($Hs \times Te$)	[45]
AWS	2.47	Point Absorber	0.5 × 0.5 ($Hs \times Te$)	[46]

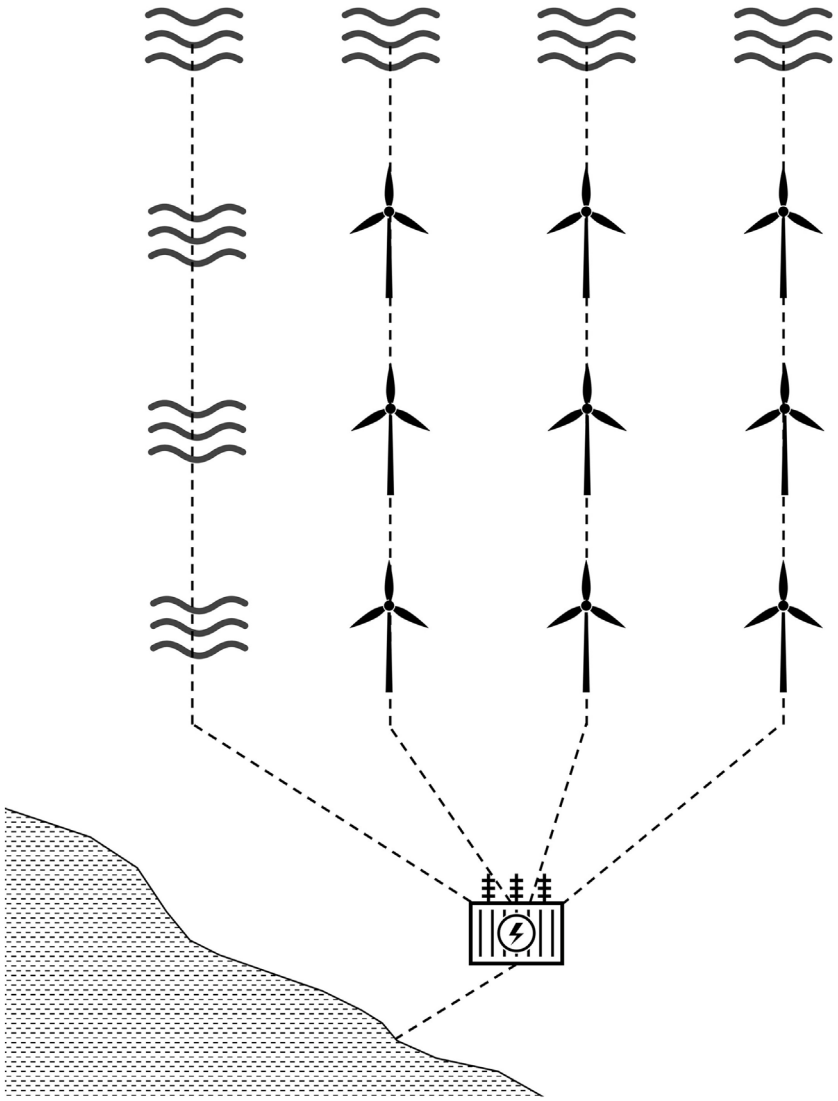

Fig. 1. Illustration of a Peripherally Distributed Array (PDA). WECs are deployed at the perimeter of the OWT array, corresponding with the dominant wave direction. Wavey parallel lines are representative of WECs and turbines of OWTs. Dashed lines represent array/export cables. Horizontal dashed area represents onshore area, and blank white space is offshore area.

reliable, publicly available power matrices [42,43]. The selected technologies offer a diverse range of designs and power matrices, enabling the evaluation of performance across a variety of wave climates. Other WECs were excluded due to limited data availability, incomplete validation, or early development stages, which would reduce the reliability of the analysis conducted within the study.

This study considers a Peripherally Distributed Array (PDA) co-located system [44]. A PDA system will deploy WECs at the perimeter of the OWT array, corresponding with the dominant wave direction, as illustrated in Fig. 1. At each site, statistical metrics were calculated with the percentage of additional capacity (deployed WECs) ranging from 0 to 100.

3. Results & discussion

3.1. Global analysis

Initially, annual mean values for Wave Power Flux (WPF) and Wind Power Density (WPD) during 2020 were calculated and plotted (Fig. 2). Similar patterns are seen by both WPF and WPD, the resources are typically larger between the subtropical high-pressure zones and the mid-latitude areas (30°–60° latitude).

The largest values of annual mean WPF and WPD are within the Southern Ocean, at 113 kW/m and 2.7 kW/m^2, respectively. More sheltered locations, such as the Gulf of Mexico, the Asia-Pacific region, and the Mediterranean Sea, exhibit reduced WPF, with values

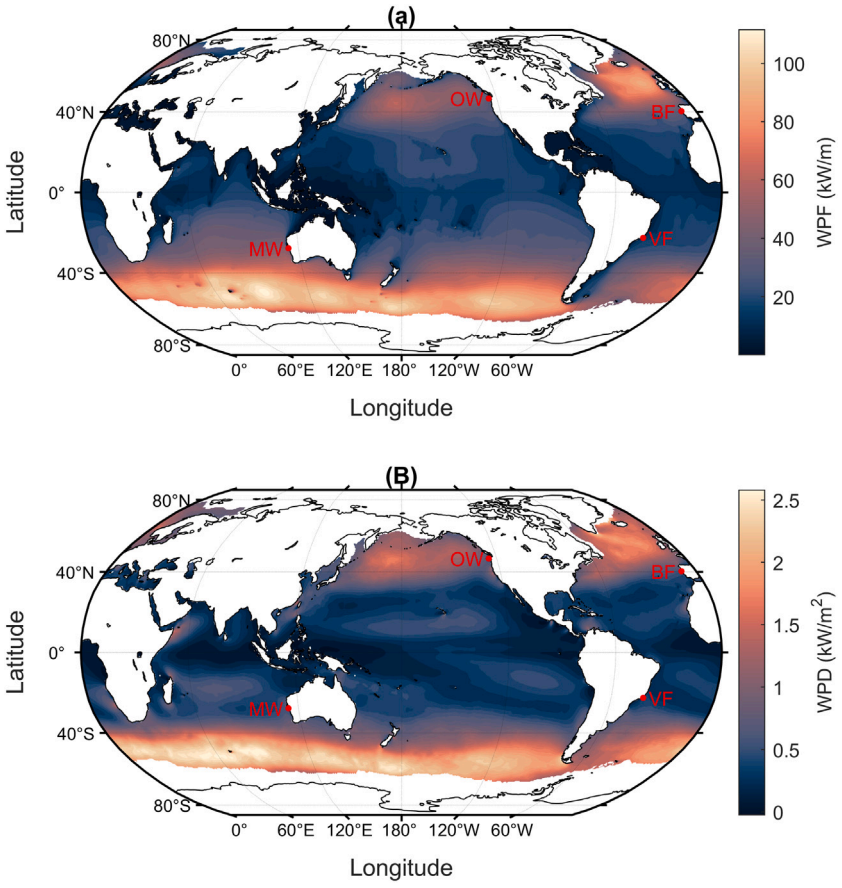

Fig. 2. Annual mean WPF (A) and WPD (B) for 2020. Calculated using 3-hourly data for the duration of 2020. The specific study array sites are shown using the labels MW (Mid-West), VF (Ventos Fluminenses), OW (Olympic Wind), and BF (Botafogo).

<6 kW/m. Reduced WPD can be observed at regions near the Intertropical Convergence Zone (5°–15° latitude), as well as other more sheltered areas, such as the Asia-Pacific region. At these locations WPD falls to <0.7 kW/m^2. The wave resource values are consistent with those calculated by Gunn and Stock-Williams [14], although covering a different time period.

Using the global WPF and WPD time series, correlation and WIWAS for each grid point were calculated (Fig. 3). Typically, exposed regions exhibit a lower correlation (R) between the WPF and WPD (<0.4), conversely, more sheltered locations exhibit a higher correlation (>0.6). Locations that exhibit a lower correlation generally have a wave climate that is dominated by swell waves, which are relatively independent of the local wind climate. In contrast, regions with a higher correlation exhibit a higher dependency on the local wind climate. This can be caused by topographical features, such as land masses, or the transition onto the continental shelf, dissipating (or refracting) the swell waves before they reach a certain region. A similar pattern, although to a lesser extent, is seen with WIWAS (Fig. 3). More exposed locations exhibit more favourable synergy (>0.8), with sheltered locations being less suitable (<0.4). Fig. 4 represents combined values for linear correlation and WIWAS, where larger values are representative of more suitable locations for co-location. As expected, more exposed locations exhibit higher suitability, whilst sheltered locations display reduced suitability.

Sites deemed suitable for combined wind/wave energy conversion were selected based upon results from Figs. 2, 3, and 4. These locations were filtered further using the 4C Offshore wind database to identify sites where wind arrays were operational, in construction, or at various stages of planning. This resulted in the selection of four specific sites for more detailed analysis.[5] Information about these study sites is summarised in Table 3.

3.2. Theoretical resource

This section expands on the estimated theoretical wind and wave resources present at each study site, using data spanning the study period 2012–2022. Fig. 5 visually compares four study sites across key metrics: linear correlation, WIWAS, WPD, and WPF. These regional plots offer an initial assessment of each site's co-location potential based on the spatial distribution of these parameters. The western coastline of Australia demonstrates strong wave and wind resources with low correlation. The southern Brazilian coastline, although wave power is relatively lower, the combination of very low correlation and high WIWAS values indicates strong complementarity between resources. The northwestern coastline of the USA, and midwestern coastline of Portugal exhibit moderate resource availability but still satisfy the criteria for viable co-location. While Fig. 5 confirms the theoretical viability of each site, the following sections (3.2.1 to 3.3.3) provide a more detailed analysis of wind and wave resources, including seasonal variations, correlation analysis, and device-specific power assessments.

[5] Botafogo (Portugal) is planned to use 18 MW turbines, this study will apply a 15 MW power curve to this site instead. This was done to enable a European comparison to other global locations, and since a reference 18 MW turbine power curve is not available.

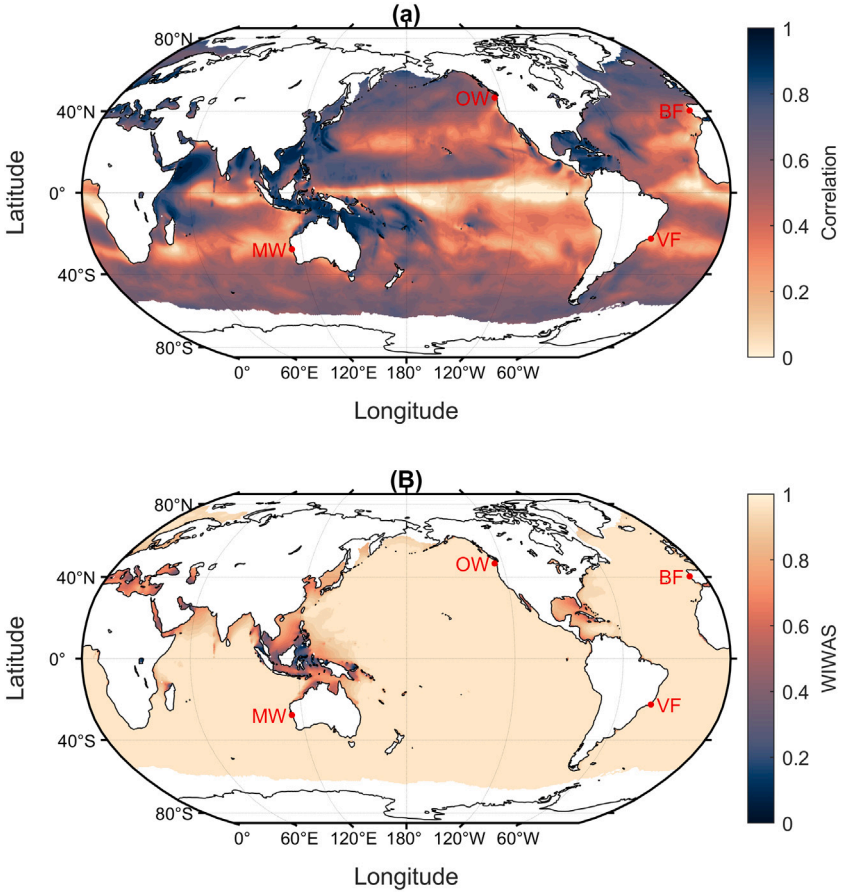

Fig. 3. Correlation (A) between WPF and WPD, and WIWAS (B). Both plots represent 3-hourly data over the duration of 2020. The specific study array sites are shown using the labels MW (Mid-West), VF (Ventos Fluminenses), OW (Olympic Wind), and BF (Botafogo).

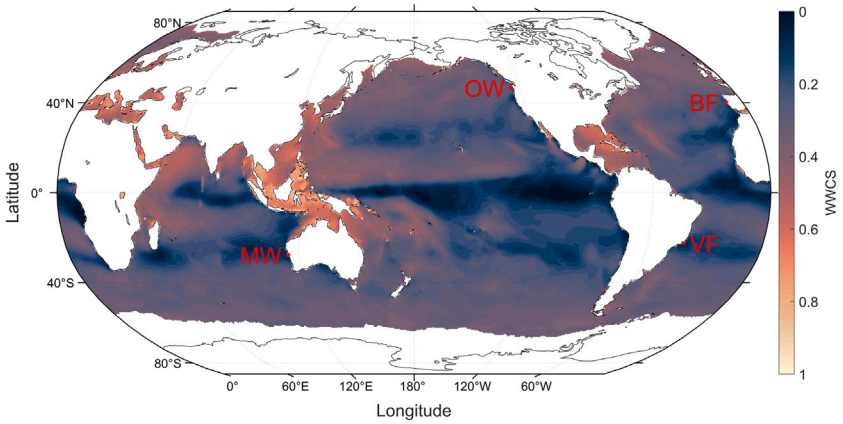

Fig. 4. Global WWCS. The plot represents 3-hourly data over the duration of 2020. Larger values are representative of more ideal locations for co-location. The specific study array sites are shown using the labels MW (Mid-West), VF (Ventos Fluminenses), OW (Olympic Wind), and BF (Botafogo).

3.2.1. Regional wind and wave resource statistics

3.2.1.1. Regional wave climates. The wave climate, and its associated Wave Power Flux (WPF), are shown in Fig. 6(a) and Fig. 6(b), respectively. Table 4 contains relevant resource statistics relating to each study site. Ventos Fluminenses presents the most concentrated range of sea states, with 0.5 m < H_s < 2.5 m and 5.0 s< T_e < 10 s. Conversely, Mid-West, Olympic Wind and Botafogo present a much broader distribution of sea states, with the latter being the most extreme case (1.5 m < H_s < 3.0 m and 7.0 s < T_e < 12.0 s, 0.75 m < H_s < 3.0 m and 5.5 s < T_e < 11.0 s, 0.5 m < H_s < 4.0 m and 5.0 s< T_e < 12.0 s, respectively).

Mid-West experiences the highest percentage of time at a more energetic state (5% at $H_s \geq 4$ m, $T_e \geq 8.5$). This is validated by Fig. 6b, the modal WPF at Mid-West is 18.1 kW/m. This trend continues for larger WPF values, with a greater percentage of time at larger WPF values compared to all other sites. Botafogo and Olympic Wind have similarly matched WPF values; however Olympic Wind experiences a

Table 3
Study sites and their associated wind array information.

Study Site	Region	OWT Array	Array Location (Lon,Lat)	Array Capacity (MW)	OWT Nominal Power (MW)	Array Status
1	Western Australia	Mid-West	114.13, −29.50	3000	15	Planning
2	Southeastern Brazil	Ventos Fluminenses	−41.6, −22.52	2820	15	Planning
3	Northwest USA	Olympic Wind	−124.5, 46.72	2000	15	Planning
4	Midwestern Portugal	Botafogo	−9.27, 40.33	990	18	Planning

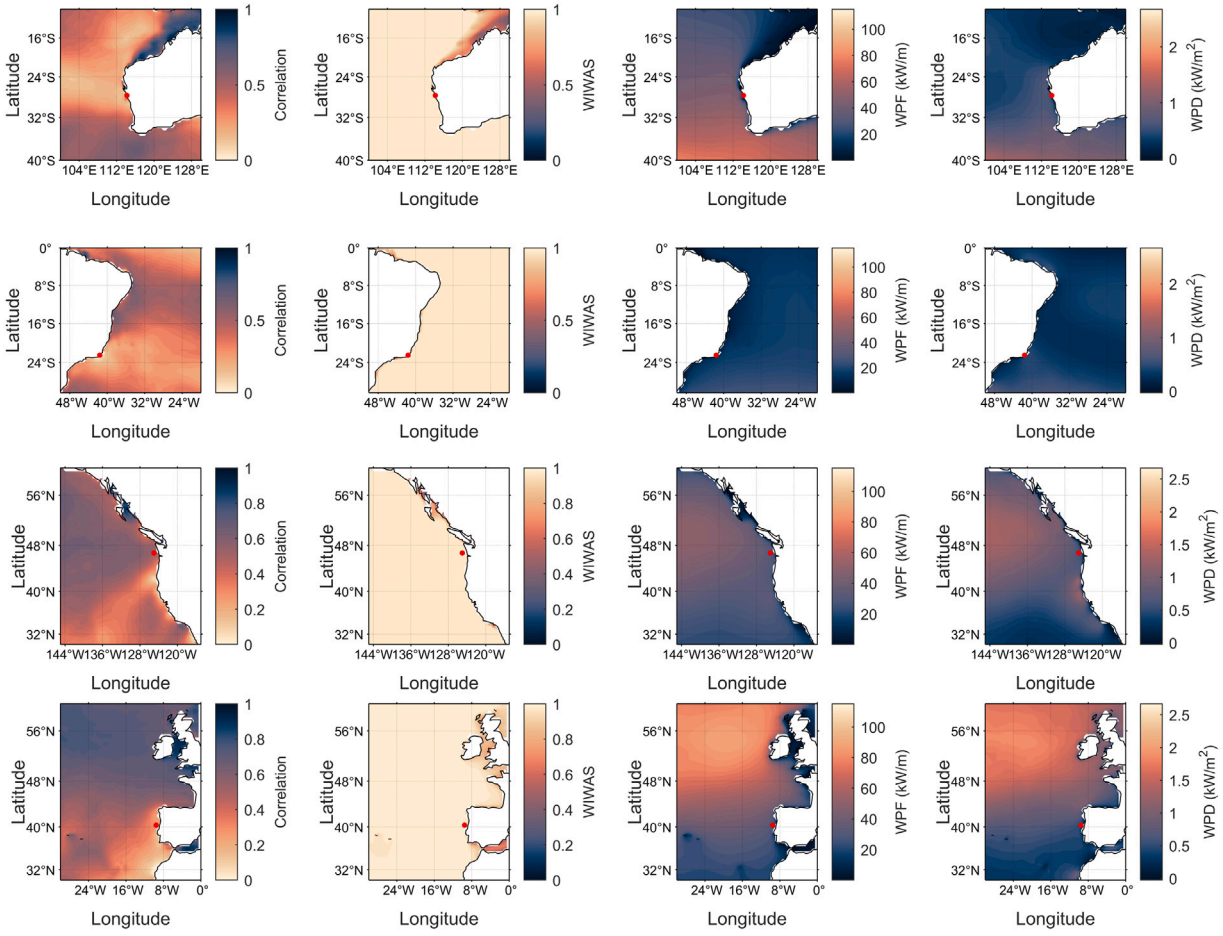

Fig. 5. Regional plots showing linear correlation, WIWAS, WPD, and WPF for each study site region: Australia (1st row), Southern Brazil (2nd row), Northwestern USA (3rd row), and Midwestern Portugal (4th row). The specific study array locations are represented by the red dot. Data spanned the study period 2012–2022.

slightly larger modal WPF at 7.6 kW/m for 7% of total time. Ventos Fluminenses has the lowest WPF resource, with a modal WPF of 6.06 kW/m. This is supported by the H_s and T_e values, as a higher percentage of time (5%) is spent at $H_s \leq 2.7$ and $T_e \geq 8.4$. The mean values in Table 4 also corroborate these findings.

3.2.1.2. Regional wind climates. The wind climate, and associated Wind Power Density (WPD), are shown in Fig. 6(c) and Fig. 6(d), respectively. Table 4 contains relevant resource statistics relating to each study site. Considering the wind states, Olympic Wind presents the least energetic resource, with a mean wind speed of 6.52 m/s. Ventos Fluminenses has a mean wind speed of 6.79 m/s. Botofogo and Mid-West are similarly matched with large wind resources (mean wind speeds of 7.53 m/s and 7.91 m/s, respectively). Botofogo does however experience the largest range of wind speeds of all four sites, with wind speed values between 3–14 m/s for >1% of total time. This results in a less stable resource, as percentage of total time remains at ≥ 0.89% for WPD 0.4–1.2 kW/m^2, a larger extent than any other site. Mid-West operates with the lowest time at zero output (7.5%) and consistently has a larger WPD output, whilst Olympic Wind has the largest percentage of time at zero output 18.4%, and generally the lowest consistent WPD.

3.2.2. Seasonal variability

Monthly averages of WPF and WPD were calculated and plotted for each study site (Fig. 7). Mid-West and Ventos Fluminenses are situated in the Southern Hemisphere, accordingly, the meteorological winter covers the months of June, July and August, and the meteorological summer covers December, January, and February. The inverse is true for Olympic Wind and Botafogo as they are situated in the Northern Hemisphere. Generally, resources were found to be more energetic during winter months and less energetic during summer months. Interestingly, this pattern does not apply to the wind climate

Table 4
Statistics relating to the wind and wave resources of each study site, over the duration of the study period (2012–2022).

Study Site	$\overline{U}$ (m/s)	$\overline{H_s}$ (m)	$\overline{T_e}$ (s)	$\overline{P}_{wind}$ (kW/m^2)	$\overline{P}_{wave}$ (kW/m)	WIWAS
Mid-West	7.908	2.612	9.813	1.08	36.578	0.969
Ventos Fluminenses	6.785	1.855	7.941	0.688	15.025	0.999
Olympic Wind	6.523	2.356	9.149	0.754	32.502	0.999
Botafogo	7.531	2.292	8.977	0.787	31.609	0.988

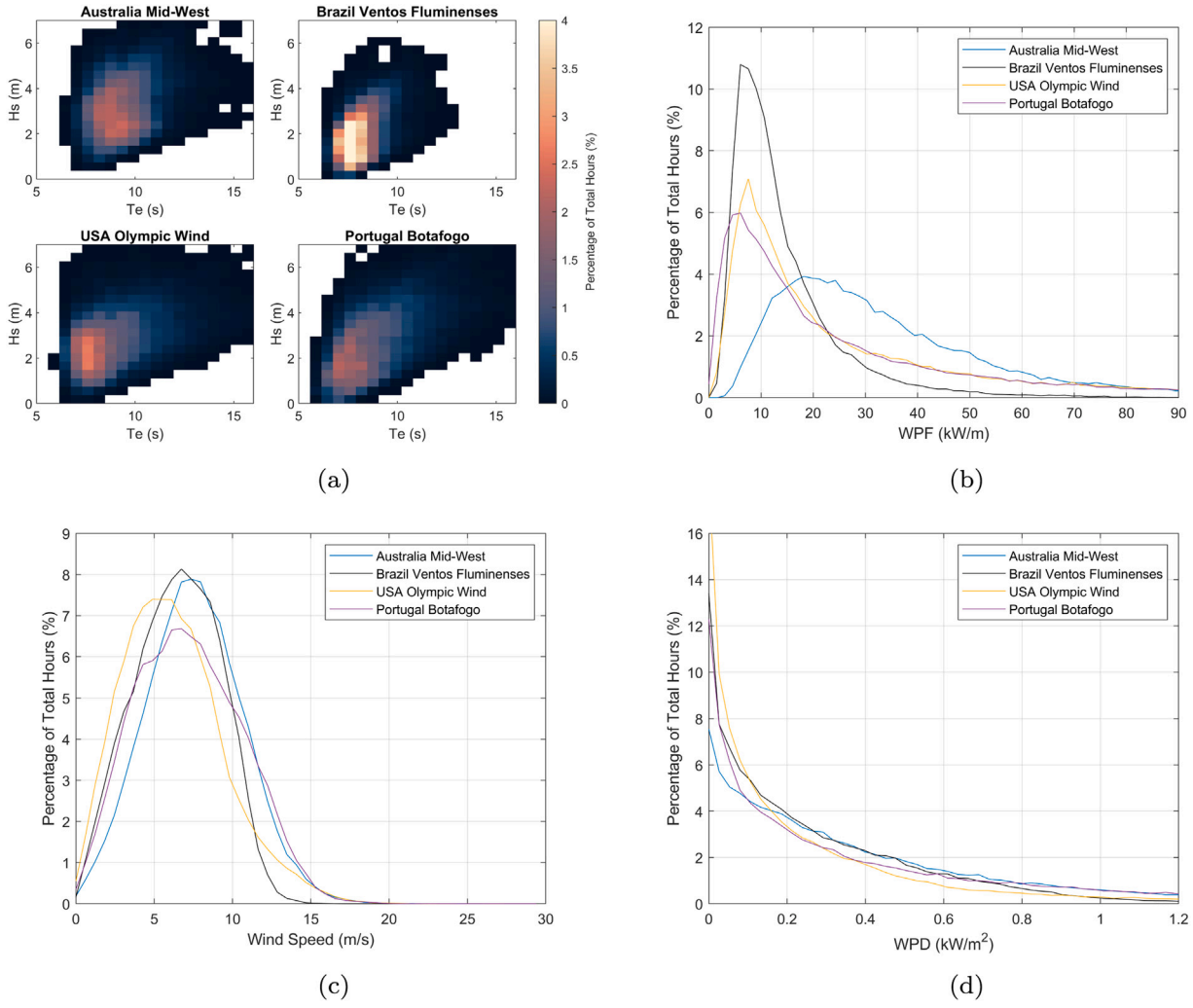

Fig. 6. Wave statistics of four sites (a) and wind speed statistics (c) of each study site for the duration of the study period (2012–2022). Their relation to WPF and WPD, respectively, is shown in (b) and (d). White space in (a) represents zero values.

of South-Western Australia (where the Mid-West array is located). Here, WPD peaks during the summer and spring months (November, December, January) at 1.44 kW/m^2, whilst the winter peak is only 1.15 kW/m^2. The West Coast Trough, a common climatic feature of Western Australia, may be the cause of this. The West Coast Trough is strongly linked to the high intensity sea breeze experienced along the South-Western coastline during summer periods; the presence of a high-pressure system to the south of Australia results in an easterly airflow across the continent, gradually warming as it travels across the continent, resulting in a low-pressure trough forming in a north–south direction [47,48]. Ventos Fluminenses experienced offset seasonal wind resource peaks and troughs; WPD peaks at 1 kW/m^2 during spring and reaches a minimum value during Autumn at 0.45 kW/m^2. This presents a promising opportunity for the joint occurrence of wind and wave energy converters as the two resources are likely to consistently complement each other on a seasonal scale; the resources peak at a different seasonal phase so the overall power output will remain more consistent.[6] Both Olympic Wind and Botafogo exhibit seasonal values which are to be expected, with both resources peaking during more energetic winter months, and troughs during calmer summer months. Fig. 7 also represents the seasonal uncertainty in both resources, denoted by the 90% confidence intervals. As to be expected, winter months exhibit larger uncertainty in both resources at all study sites; more dynamic and variable atmospheric and oceanic conditions

[6] The effect of seasonal phasing when considering co-location can only be fully understood by analysing long-term data trends. While the technical resource analysis (Section 3.3) considers the entire study period, it relies on statistical representations that do not explicitly resolve seasonal-scale effects. Identifying these longer-term trends requires direct visualisation of data over extended timescales.

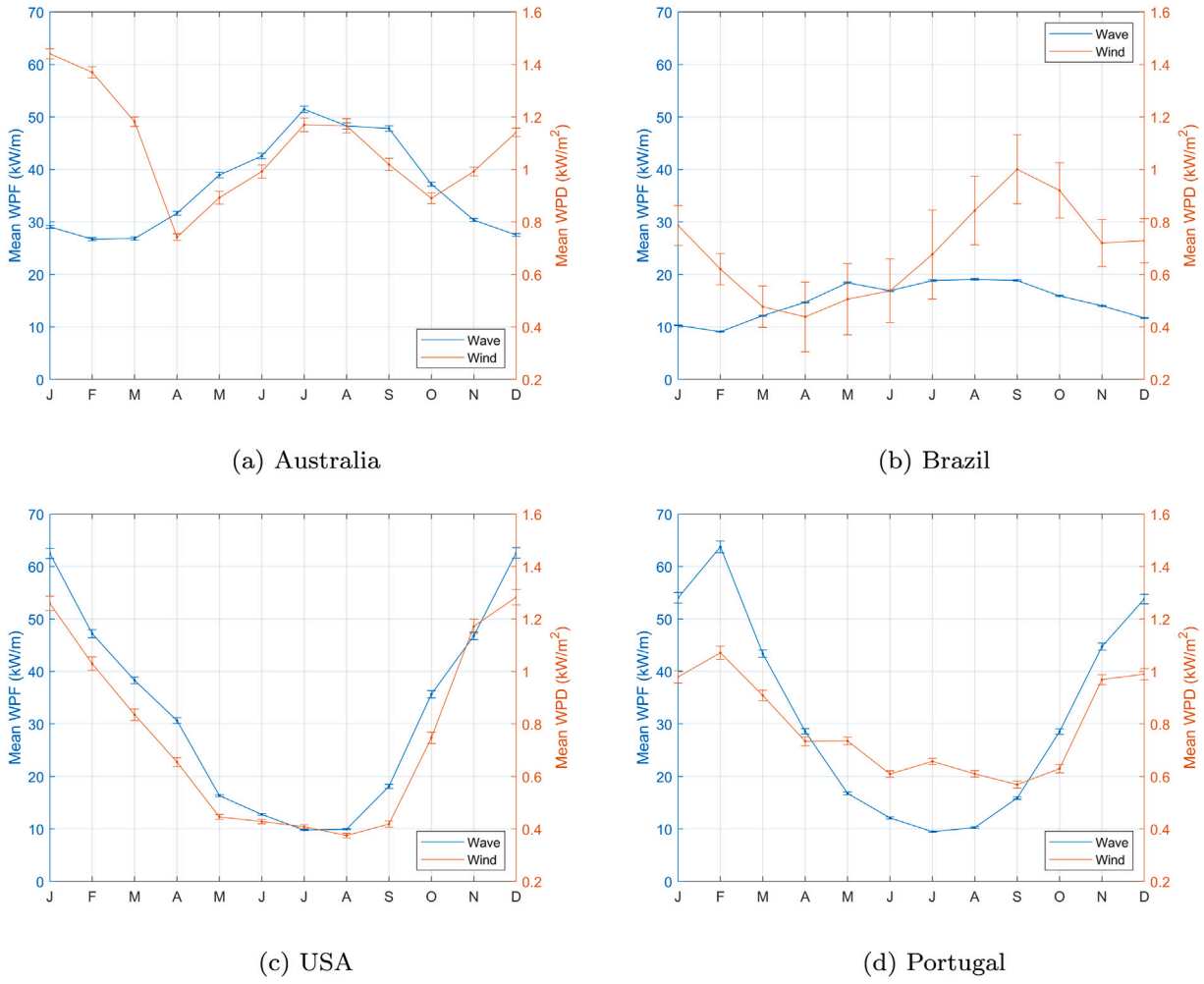

Fig. 7. Monthly mean WPF (blue) and WPD (orange) for each study site based on 11 years of model analysis (2012–2022): Mid-West (a), Ventos Fluminenses (b), Olympic Wind (c), and Botafogo (d). Error bars represent 90% confidence intervals. X-axis represents months of the year.

operate during these months, increasing the extremes, resulting in an overall less stable resource. The larger confidence intervals at Ventos Fluminenses indicate a significantly more unstable wind resource across all months; with the 90% confidence intervals circa ±0.2 kW/m^2.

3.2.3. Resource correlation

The correlation, and associated time lag, between the wind and wave resource at each study site is shown in Table 5 and illustrated in Fig. 8, calculated over the entire study period (2012–2022). All study sites present feasible correlation conditions for co-located wind and wave energy conversion. Ventos Fluminenses presents the strongest potential for co-location as it represents the lowest correlation between resources (C(0) = 0.202). This will likely result in sufficient power smoothing, as the two resources are generally out of phase with one another. Mid-West displays similar potential, with a low correlation of C(0) = 0.204. Botafogo displays modest potential with C(0)=0.438. Olympic wind experiences the highest correlation of C(0)=0.562. This larger correlation may cause issues for a combined array, as power output variability might not be reduced. However, it is not significant enough to disregard Olympic Wind as a potential site for co-location.

Resource correlation can be illustrated further using a joint probability plot which shows the relationship between WPF and WPD, and the percentage of time spent at each value (Fig. 9). Time periods with large WPF do not frequently correspond to periods of large WPD, representing low correlation, and suitable scenarios for co-location.

The correlation values are largely comparable with those found in other studies. Gao et al. [20] identified that Cliff Head (Mid-Western Australia) presented strong potential for the co-location of WECs and OWTs. C(0) was found to be 0.21, a value consistent with this study (C(0) = 0.202). Fusco et al. [25] identified that the western coast of Ireland presents a strong opportunity for co-location. At this location, C(0) was calculated to be 0.1, with $C_{max}(\tau)$ 0.356 at 10 h. This suggests that Western Ireland could potentially serve as a more ideal co-location site within Europe than the Botofogo site selected within this study, due to its more optimised resource phasing. Neill [23] identified the co-location potential within the Celtic Sea. Across the 10 year study period C(0) was found to be 0.502, with a τ of 3 h. The Celtic Sea offers moderate potential for co-location, however the Botafogo site presented in this study, and Western Ireland [25], offer stronger potential for a European co-location site. Other aspects, such as grid connectivity and suitable ports to facilitate construction, are also important, and need to be considered when evaluating an optimal site for co-location. Gideon et al. [49] identified resource phasing characteristics along the US Californian coastline. C(0) values were found to be 0.439, with $C_{max}(\tau)$ 0.451 at 1 h. The Californian coastline and Washington coastline (Olympic Wind) display similar correlation values, however Olympic Wind operates with larger phase shift between resources ($C_{max}(\tau)$ at 5 h), so could represent a more ideal site for co-location along the US West Coast. Wen et al. [21] identified potential sites for co-location within the Taiwan Strait. These sites had C(0) values ranging between 0.6–0.7, this would likely provide an unstable resource due to the strong phasing between wind and waves; all locations analysed within this study present more favourable resource phasing, and so suggest a stronger potential for co-location.

Table 5
Correlation between WPD and WPF at each study site for the duration of the study period (2012–2022). $C(0)$ represents instantaneous cross-correlation, $C_{max}(\tau)$ represents the maximum cross-correlation coefficient at time lag τ, in hours.

Study Site	C(0)	$C_{max}(\tau)$	τ(h)
Mid-West	0.204	0.386	22
Ventos Fluminenses	0.202	0.223	4
Olympic Wind	0.562	0.611	5
Botafogo	0.438	0.473	6

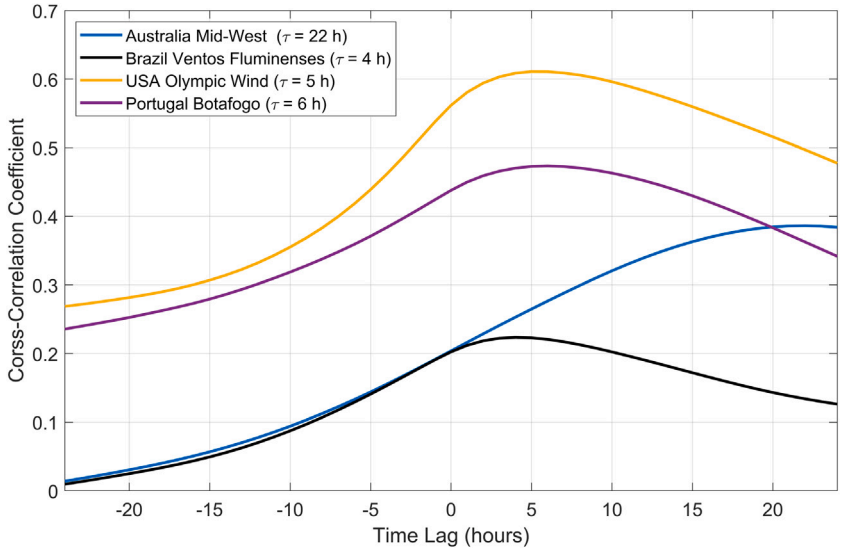

Fig. 8. Cross-correlation and their associated time lag between WPD and WPF at the four study sites.

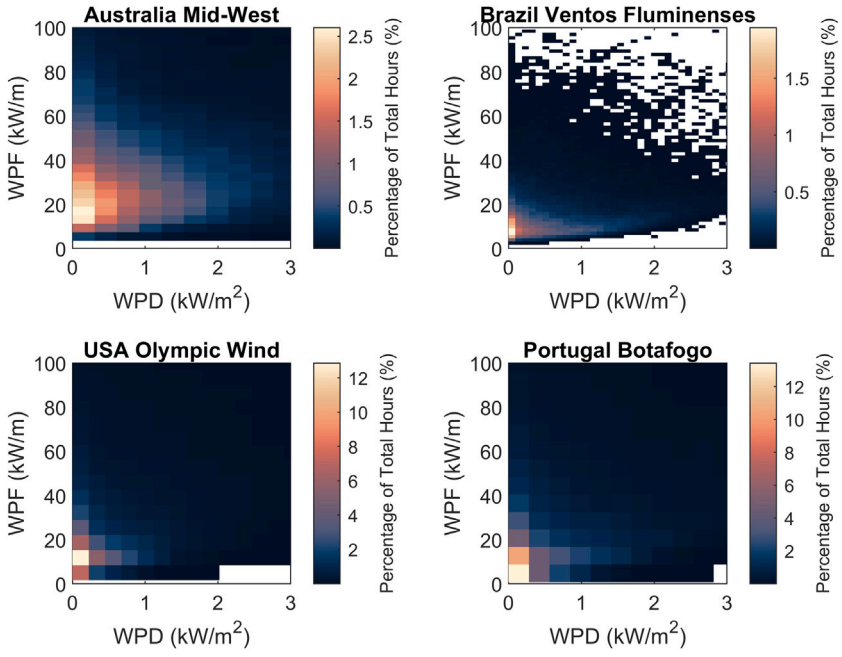

Fig. 9. Joint probability estimates of WPD and WPF at the four study sites. More energetic sea states are not highly correlated with larger values of wind power. White spaces are representative of zero values.

3.3. Technical resource

For a more thorough understanding of the suitability each site has to the joint occurrence of wind and wave energy conversion, the power curves of OWT and power matrices of WEC devices need to be applied. In each case, the suitable OWT is employed (as specified in Table 1), then various WEC devices are applied (see Table 2), 'topping-up' (i.e. augmenting) the capacity of each study site OWT array. The

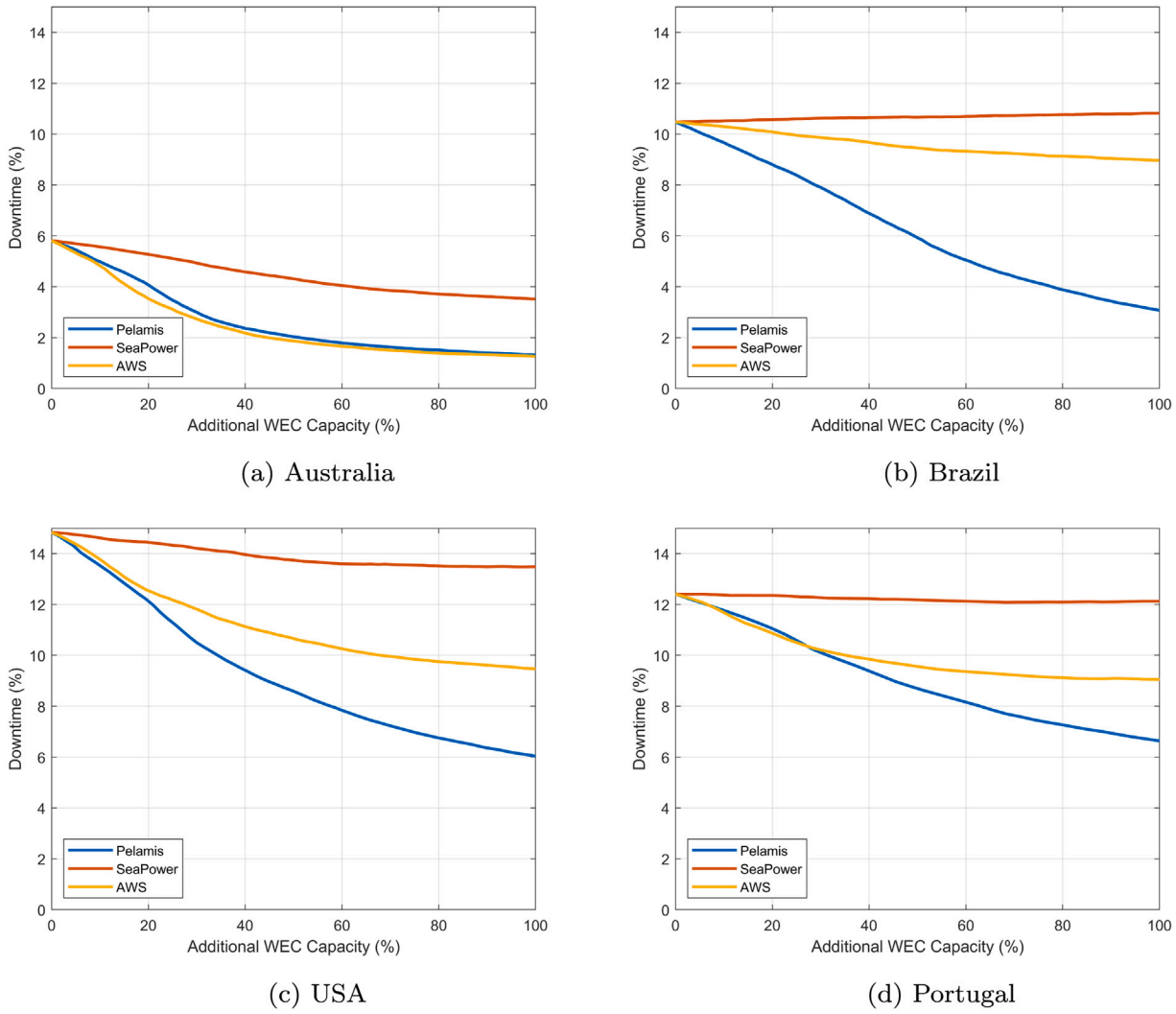

Fig. 10. Downtime against the percentage of additional WEC capacity added (compared to linked OWT array), for four different WEC devices at four different study sites: Mid-West (a), Ventos Fluminenses (b), Olympic Wind (c), and Botafogo (d). Downtime is expressed as a percentage, with downtime being equal to any output values below 5% of the installed capacity.

effect of this on variability and downtime are explored in this section, including sensitivity analysis between WEC technologies.

3.3.1. Downtime

Apart from cost reduction through shared infrastructure, one of the overall motivations for co-located wind-wave energy conversion is the development of a more consistent and stable power resource. This not only includes reduced variability, but more generally, reduced array downtime due to lulls in the resource, which is particularly an issue with renewable energy resources [20]. Downtime is considered as the percentage of time total power output is below 5% of the installed capacity [20]. The results of this are found in Fig. 10. As to be expected, downtime generally reduces as WEC capacity is added, except for SeaPower WEC at Ventos Fluminenses, which marginally increased downtime. Ventos Fluminenses operates with the highest proportion of time spent at reduced H_s and T_e values, and thus, lower WPF values (Table 4). This characteristic, when combined with the Sea Power WEC matrix results in highly inefficient power production; SeaPower requires a higher proportion of time spent with $T_e > 9.5$ s and $H_s > 4$ m for a higher capacity factor to be achieved. This is the likely cause for downtime increase at Ventos Fluminenses when SeaPower WEC capacity is added. Other locations operate with a higher proportion of time at larger H_s and T_e, so experience more efficient energy conversion with Sea Power WEC. Once again, Mid-West displayed the lowest downtime of 1.25% for 100% of additional wave energy capacity. Olympic Wind has the largest total reduction in downtime; 8.3% for 100% of additional capacity. Ventos Fluminenses has the second lowest downtime at 3%, although Mid-West experiences a higher rate of change, with a larger reduction experienced between 0%–40% additional WEC capacity. Botafogo downtime reduces to a minimum of 6.8% at 100% additional capacity. Pelamis and AWS devices are generally evenly matched at all sites, except for Ventos Fluminenses where Pelamis outperforms AWS. SeaPower is consistently the worst performer across all study sites. Interpretation of these performances is expanded upon further in 3.3.3.

3.3.2. Variability

The CoV for each study site, with increasing additional capacity of WEC devices, can be found in Fig. 11. At all study sites, increased WEC capacity reduced CoV, meaning the overall output was more stable, and less variable. Mid-West displays the lowest CoV, at 0.417; this is representative of the largest reduction in variability (17%). Ventos

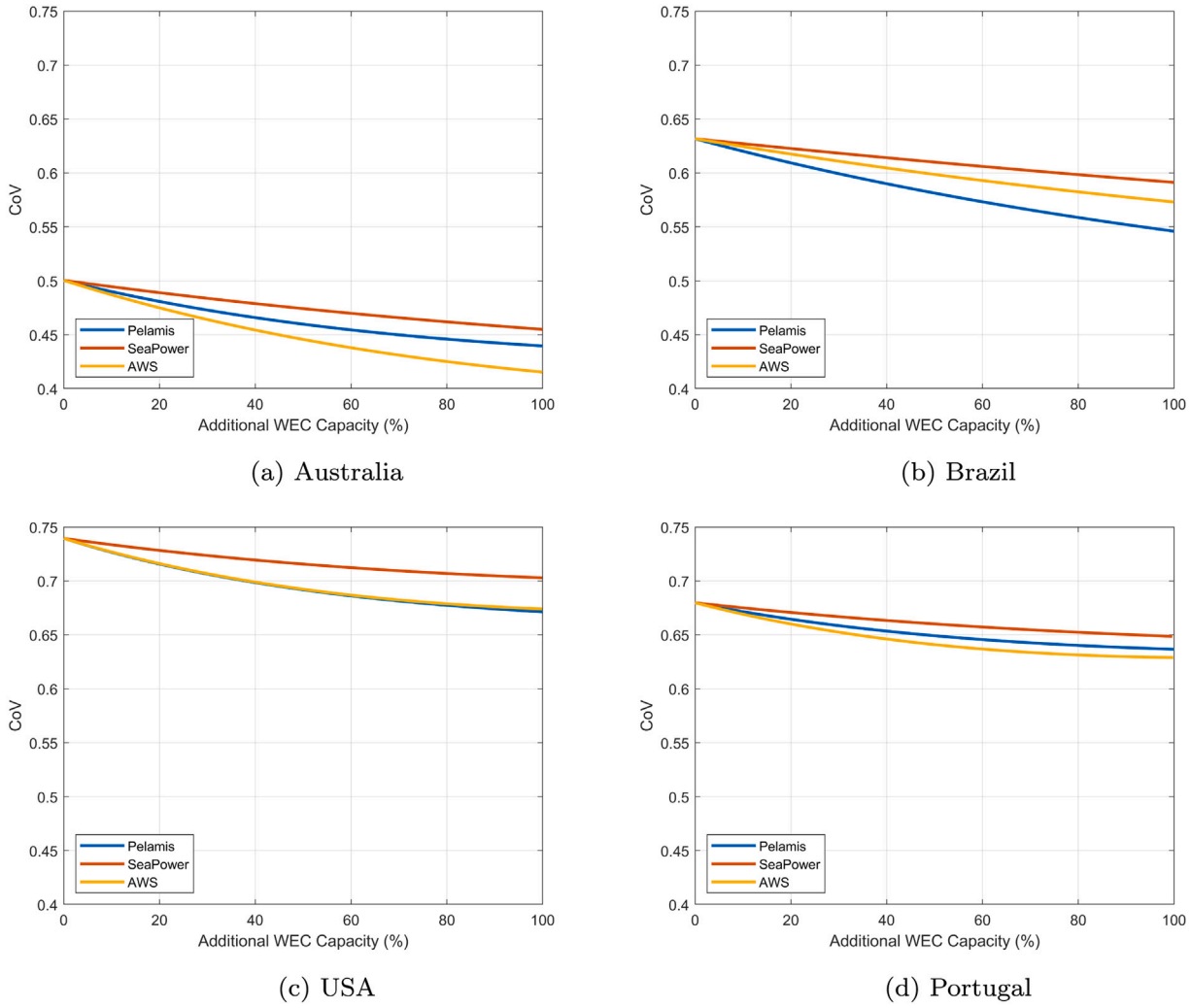

Fig. 11. Coefficient of Variability (CoV) against the percentage of additional WEC capacity added (compared to linked OWT array), for four different WEC devices at four different study sites: Mid-West (a), Ventos Fluminenses (b), Olympic Wind (c), and Botafogo (d). The different WEC devices are shown in the legend.

Fluminenses and Botafogo operate with similar variability performance. However, when WEC capacity is added, Ventos Fluminenses displays much stronger performance, with a reduction in CoV of 13%, compared to only 6% at Botafogo. Olympic Wind operates in the middle ground, with a CoV reduction of 9%. These values were achieved using Pelamis WEC (Ventos Fluminenses and Olympic Wind) and AWS WEC (Mid-West and Botafogo), at 100% additional capacity; Wave energy is a much less variable resource at these sites. There are diminishing returns as the percentage of additional WEC capacity increases, the highest rate of change (steepest gradient) is between 0%–10% of additional capacity, gradually declining until the midpoint at 50%. Beyond this point, return on additional installation of WEC devices begins to taper off. Interpretation of these performances is expanded upon further in 3.3.3.

Understanding the achievable technical resource on an intra-annual scale can also assist the perception of combined resource variability. Fig. 12 illustrates the monthly means for combined and stock (wind-only) arrays. These averages have been normalised based on the site-specific mean output, enabling comparison regardless of the array capacity. Combined arrays are representative of the stock OWT array, supplemented by an additional 50% Pelamis capacity. Pelamis was selected based on its extensive ocean testing and its more common use across literature and 50% was selected as a midpoint representation to illustrate the general effects of co-location on intra-annual variability without biasing towards either end of the capacity scale. Mid-West, Ventos Fluminenses and Botafogo become more stable, with most values closer to the mean throughout the year. Botafogo exhibits the lowest overall seasonal variability, with combined output remaining within ±0.12 of the mean. Mid-West similarly performs well, with a maximum variance of ±0.21. Ventos Fluminenses performs strongly during January–July, with values being closer to the mean and more stable. During the second half of the year (August–December) the additional WEC capacity has little impact on variance. Olympic Wind performs less effectively when WEC capacity is added during the summer but shows improved performance in the winter. This is due to the rate of resource change experienced at this scale (see Fig. 7). During the winter, the wind resource has a larger relative change than the wave resource over this temporal period (i.e. it is more variable). Conversely, during the summer, the wind resource is more stable, and so will have less variance than the combined array over this time period. The results presented in Fig. 12 are largely to be expected; a combination of the intra-annual WPF and WPD values (Fig. 7). There is minimal change in variance when there is a strong positive correlation, however when the site displays a negative/zero correlation, variance is reduced.

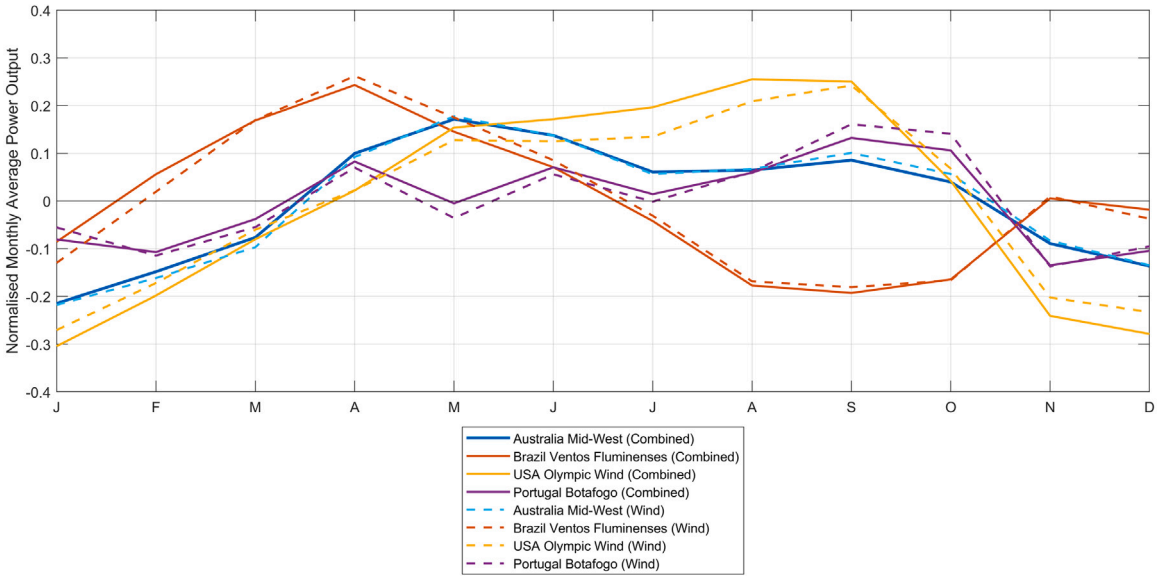

Fig. 12. Normalised monthly power output for combined arrays (solid line), and stock wind-only arrays (dashed line) for multiple study sites. *X*-axis represents months of the year. Data analysis was completed over the entire study period (2012–2022). Values are normalised based on the site-specific mean power output. Values closer to zero are indicative of a more stable power resource.

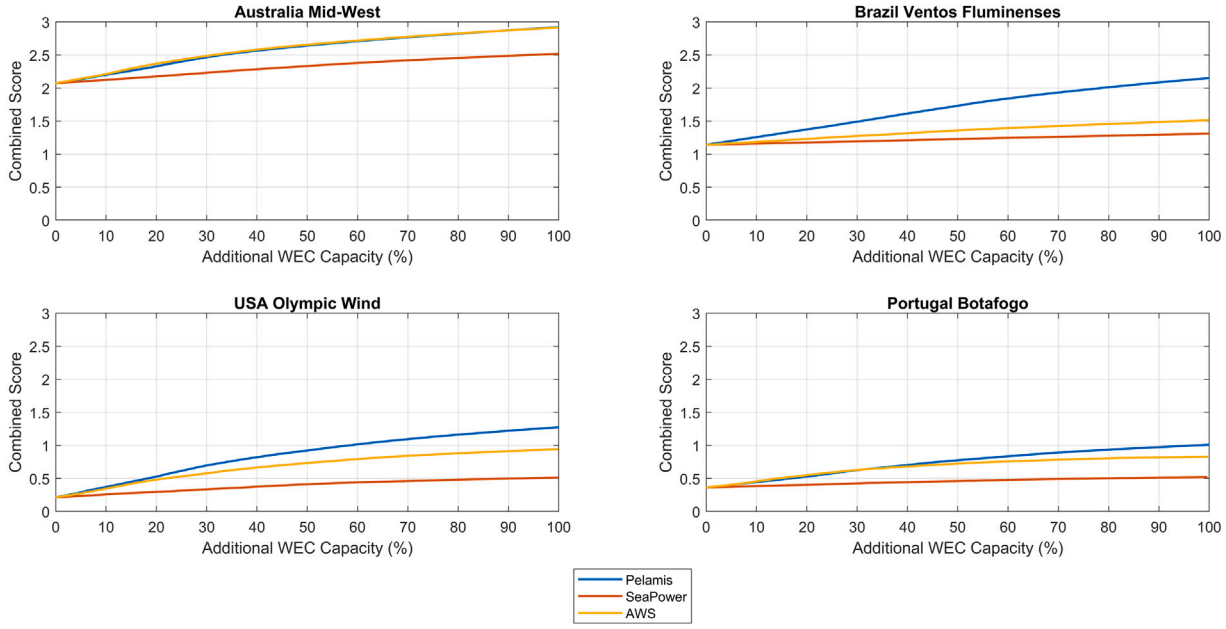

Fig. 13. Performance of four WEC devices, at four different study sites. Larger combined score is representative of a stronger performing WEC array. Values are expressed at a percentage of additional WEC capacity (compared to linked OWT array).

3.3.3. WEC sensitivity analysis

OWT development and commercial optimisation has led to their design converging on a horizontal axis, three twisted-blade configuration [50]. Due to their common design, device power curves are largely consistent. Conversely, WEC design is broadly spread, with multiple technology types (e.g. point absorber, attenuator, terminator) currently being developed. Therefore, a sensitivity analysis is conducted to understand the optimum WEC device for the specific sea state of each study site, and which percentage of additional capacity represents the most effective array capacity-performance ratio. Fig. 13 shows how the performance of the four WEC devices varies by site as additional WEC capacity is added (expressed as a percentage increase). Performance is represented by a composite score that combines three metrics: coefficient of variation (CoV), downtime, and mean total output. Each metric is normalised to a 0–1 scale based on its range across all devices at each site, where 0 indicates the worst and 1 the best performance. The normalised metrics are then equally weighted and summed to produce the final score. Pelamis and AWS typically have similar performance across most sites at lower percentages of additional capacity, with the exception of Ventos Fluminenses, where Pelamis consistently outperforms AWS. Pelamis operates with stronger performance at larger percentages of additional capacity, except for Mid-West, where they remain evenly matched. The larger performance

gap seen between Pelamis and AWS at Ventos Fluminenses is due to the specific sea state present at that location; more quiescent wave climates enable devices to operate at a higher capacity factor (see Figs. 6(a), A.2, A.3) and will therefore display better performance at that site. The slight stronger performance of AWS at Mid-West is due to a similar reason; the more energetic wave climate enables AWS to operate at a higher capacity factor, resulting in stronger performance. SeaPower is consistently the weakest performer at all study sites, at all percentages of additional capacity, and is not recommended for deployment at any of the selected sites. Higher performing alternatives present a more feasible option. This poor performance is a direct consequence of the reduced operating window for larger capacity factors (Fig. A.4). The performance of the WEC device is largely due to the specific availability of capacity factor across sea states, and not due to the technology type (attenuator, point-absorber, etc.) as each WEC device tested operated over approximately the same range of H_s and T_e, however a broader range of WEC devices, including more of each classification would need to be tested for a more definitive conclusion. It is recommended that each site deploys at least 30% additional capacity; although technical performance continues to improve with additional WEC capacity up to 100%, the rate of improvement significantly decreases beyond 30%–50%. Given the current cost and maturity limitations of WECs, we recommend up to 30% additional capacity as a practical balance between performance gain and deployment feasibility.

All sites presented in this study would be suitable for the joint occurrence of wind and wave energy conversion, with the total power output of each array becoming more stable as WEC capacity is added (reduced downtime and variability). However, some sites present a more effective optimisation of the combined resources than others. Mid-West (Australia) offers the strongest case for co-located wind-wave energy conversion, representing the lowest CoV and downtime, joint lowest C(0), largest time lag, and largest combined score. Olympic Wind (US Pacific) shows the largest performance increase; its combined score increased by a maximum of 1.7, owing to its significant reduction in downtime and CoV, so should strongly be considered for co-location. Ventos Fluminenses and Botafogo display sufficient maximum performance gains, via a reduction in downtime and CoV, of 1.34 and 1.07, respectively.

4. Conclusion

This study has presented an analysis of the benefits to the joint occurrence of wind-wave energy converters at four different global locations. ERA5 has been used to source temporal and spatial data relating to global wind and wave climates. Statistical metrics, such as linear correlation, cross correlation, variability, and synergy were calculated to gauge the suitability of each study site (with contrasting wind and wave climates) to the joint occurrence of wind-wave energy conversion. A sensitivity analysis of WEC technologies to each sea state was also conducted using the power matrices of four different WECs. The Mid-West OWT array in Western Australia was concluded as the most suitable site for co-located conversion, owing to its low correlation, and large time lag between resources. These suitable characteristics are driven by the swell driven wave climate, together with the typical wind seasonal profile, at the Mid-West OWT array in Western Australia. When WEC capacity was added to the array, it also displayed the lowest downtime and variability, indicating a more stable total power output. The Olympic Wind array in Northwestern USA showed the strongest improvement in overall performance compared to its baseline when WEC capacity was added; Olympic Wind had the greatest change in downtime and saw a large decrease in variability. Botafogo in Midwestern Portugal, and Ventos Fluminenses in Southeastern Brazil both performed sufficiently, with overall array performance increasing at both sites when WEC capacity was added. The Southern hemisphere sites displayed strong potential at the instantaneous and seasonal scales; both Mid-West and Ventos Fluminenses had seasonally offset peaks in resource phase. Conversely, the high latitude northern hemisphere sites (Botafogo and Olympic Wind) show potential due to instantaneous differences from a swell driven wave climate.

AWS and Pelamis both performed similarly at the Mid-West array, however Pelamis outperformed AWS at all other sites as Pelamis was able to operate at higher capacity factors at these less energetic sites. SeaPower regularly performed the weakest across all sites, a direct consequence of the reduced operating window for larger capacity factors.

This study presents itself as a framework for the analysis into the joint-occurrence of wind-wave energy converters at sites across the globe. The use of the ERA5 dataset enables this study to be replicated at any location on Earth. The power matrix of any WEC or power curve of any OWT can be applied, so the implications of joint occurrence can be understood considering any WEC/OWT combination. The use of a 'topping-up' approach has enabled a more effective understanding of the achievable benefits to the joint occurrence of converters. The current economic feasibility of WECs is such that the only method of widespread commercial implementation is via offsetting their cost using OWT arrays. Furthermore, the widespread implementation of WECs will likely significantly accelerate their development, on account of the economic incentive.

However, this study does contain limitations, and possible targets for future research. This study does not present metrics relating to the economic costing of technologies, and the associated market/supply chain; factors that will likely have a stronger weighting on the feasibility of co-located arrays. This study does not account for the wake effect caused by multiple turbines within proximity of each other, farm layout, and other logistical considerations. These factors are likely to greatly impact power availability. Furthermore, this study only considers prototype OWTs and WECs, for a more accurate representation of co-located wind-wave energy conversion performance, more up-to-date power matrices should be used. Furthermore the resolution of the ERA5 dataset could introduce some inaccuracies, particularly considering the nearshore environment. This is important when applying other WEC technology types, such as overtopping WECs (e.g. WaveDragon [51]), so additional validation will be required. Future research should adopt the approach taken in this study, but focus on these limitations.

CRediT authorship contribution statement

Aidan Sewter: Writing – review & editing, Writing – original draft, Conceptualization. **Simon P. Neill:** Writing – review & editing, Supervision, Conceptualization.

Declaration of competing interest

The authors declare that they have no known competing financial interests or personal relationships that could have appeared to influence the work reported in this paper.

Appendix

See Figs. A.1–A.4.

Data availability

Full information relating to the ERA5 dataset used can be found here https://cds.climate.copernicus.eu/cdsapp#!/dataset/reanalysis-era5-single-levels?tab=form. The wave energy power matrices are presented in the appendix, and the wind power curve can be downloaded here https://nrel.github.io/turbine-models/IEA_15MW_240_RWT.html.

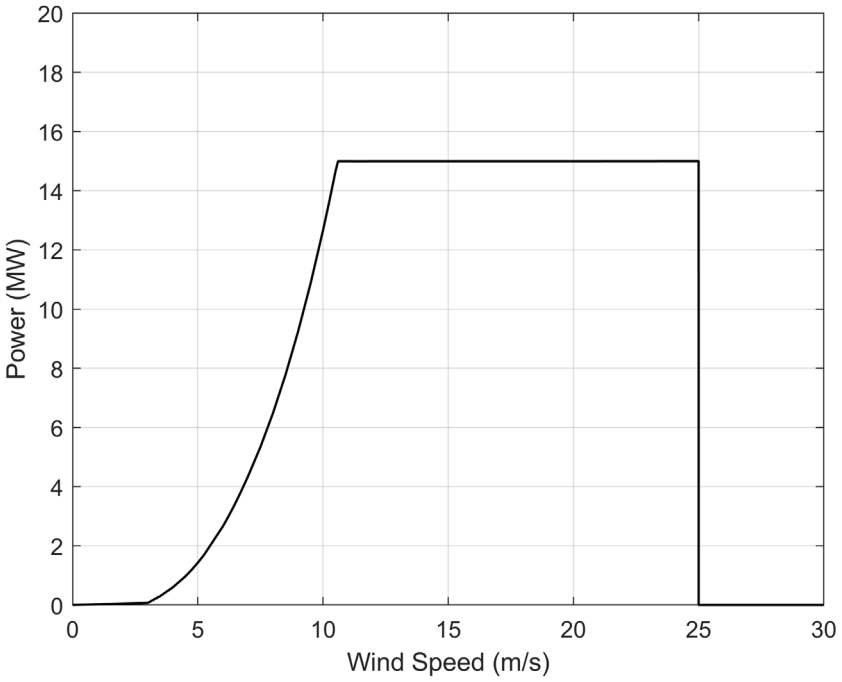

Fig. A.1. Power curve of IEA reference 15MW OWT. From Gaertner et al. [39].

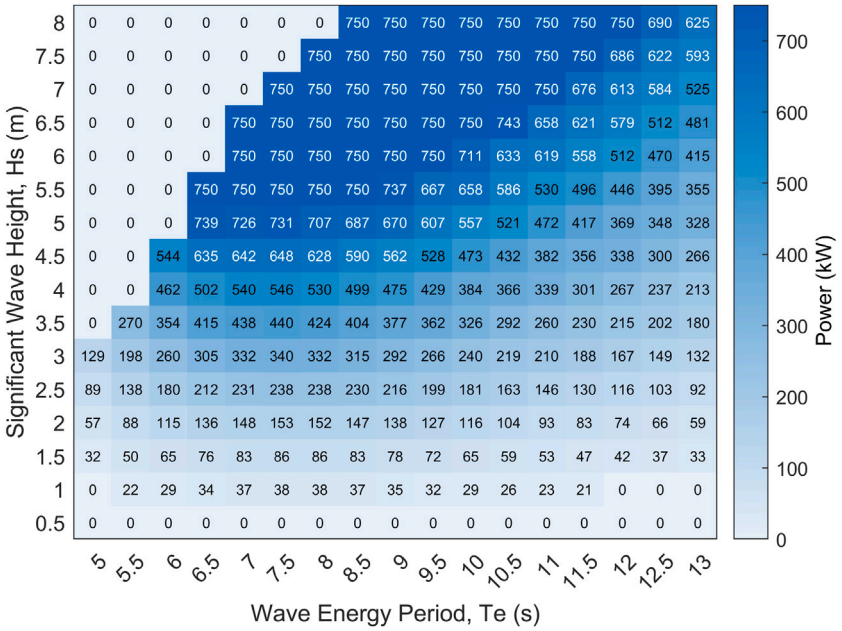

Fig. A.2. Pelamis power matrix. Power values are in kW. From Bozzi et al. [43].

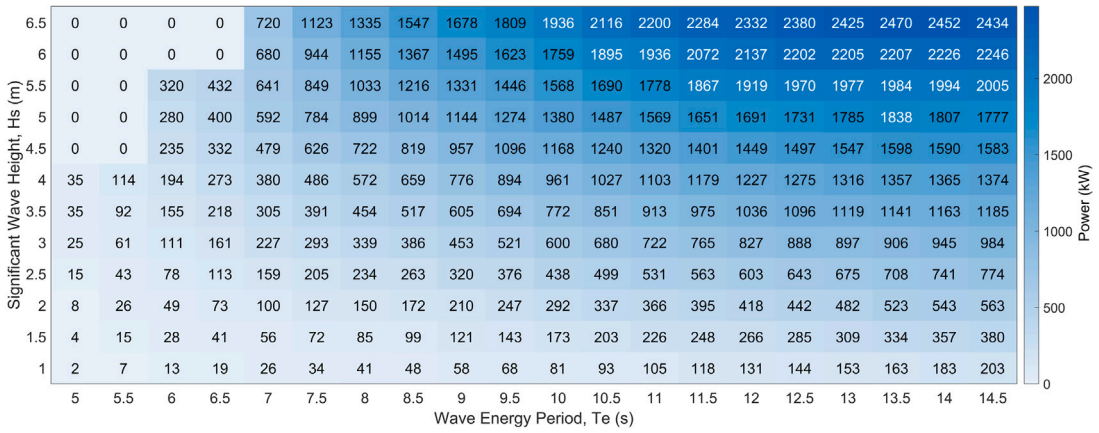

Fig. A.3. AWS power matrix. Power values are in kW. From Sinden [46].

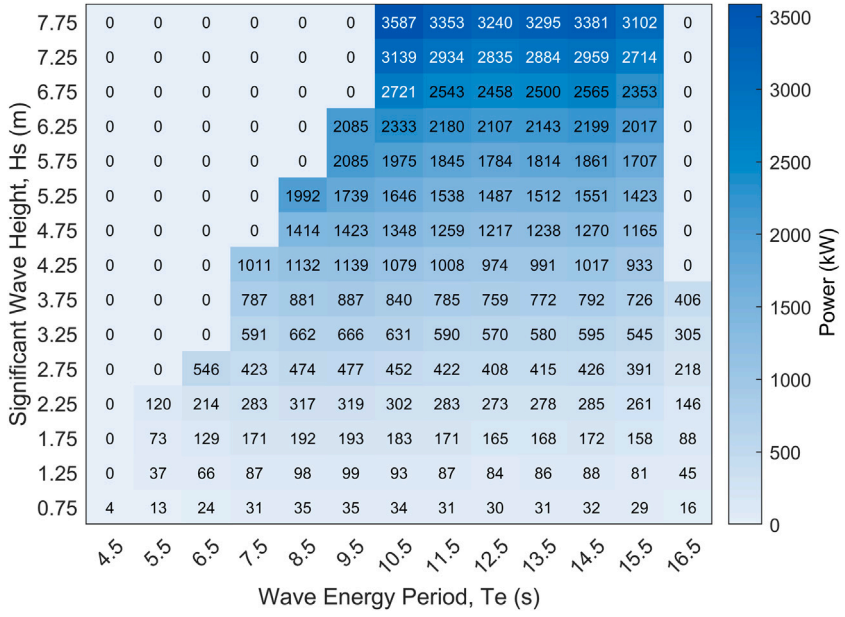

Fig. A.4. SeaPower power matrix. Power values are in kW. From SeaPower [45].

References

[1] COP26, COP26 explained, 2021, URL https://ukcop26.org/. Online; (Accessed 13 February 2023).

[2] UNFPA, World population dashboard, 2023, URL https://www.unfpa.org/data/world-population-dashboard. Online; (Accessed 28 May 2023).

[3] N. Bento, M. Fontes, Emergence of floating offshore wind energy: Technology and industry, Renew. Sustain. Energy Rev. 99 (2019) 66–82, http://dx.doi.org/10.1016/j.rser.2018.09.035.

[4] J. Shuai, Y. Zhao, Y. Wang, J. Cheng, Renewable energy product competitiveness: Evidence from the united states, China and India, Energy 249 (2022) 123614, http://dx.doi.org/10.1016/j.energy.2022.123614.

[5] GWEC, Global Offshore Wind Report 2024, 2024, URL https://gwec.net/global-offshore-wind-report-2024/.

[6] H.C. Bloomfield, D.J. Brayshaw, L.C. Shaffrey, P.J. Coker, H.E. Thornton, The changing sensitivity of power systems to meteorological drivers: a case study of Great Britain, Environ. Res. Lett. 13 (5) (2018) 54028.

[7] S.M. Fisher, J.T. Schoof, C.L. Lant, M.D. Therrell, The effects of geographical distribution on the reliability of wind energy, Appl. Geogr. 40 (2013) 83–89, http://dx.doi.org/10.1016/j.apgeog.2013.01.010, URL https://www.sciencedirect.com/science/article/pii/S0143622813000374.

[8] H.E. Thornton, A.A. Scaife, B.J. Hoskins, D.J. Brayshaw, The relationship between wind power, electricity demand and winter weather patterns in Great Britain, Environ. Res. Lett. 12 (6) (2017) 64017, http://dx.doi.org/10.1088/1748-9326/aa69c6.

[9] A. Bisercic, U. Bugaric, Reliability of Baseload Electricity Generation from Fossil and Renewable Energy Sources, Energy Power Eng. 13 (2021) 190–206, http://dx.doi.org/10.4236/epe.2021.135013.

[10] B. News, Nord stream 1: How Russia is cutting gas supplies to europe, 2022, URL https://www.bbc.co.uk/news/world-europe-60131520. Online; (Accessed 31 August 2023).

[11] Z. Wang, R. Carriveau, D.S.-K. Ting, W. Xiong, Z. Wang, A review of marine renewable energy storage, Int. J. Energy Res. 43 (12) (2019-10-10) 6108–6150, http://dx.doi.org/10.1002/er.4444.

[12] M. Lewis, J. McNaughton, C. Márquez-Dominguez, G. Todeschini, M. Togneri, I. Masters, M. Allmark, T. Stallard, S. Neill, A. Goward-Brown, P. Robins, Power variability of tidal-stream energy and implications for electricity supply, Energy 183 (2019) 1061–1074, http://dx.doi.org/10.1016/j.energy.2019.06.181.

[13] S.P. Neill, A. Angeloudis, P.E. Robins, I. Walkington, S.L. Ward, I. Masters, M.J. Lewis, M. Piano, A. Avdis, M.D. Piggott, G. Aggidis, P. Evans, T.A.A. Adcock, A. Židonis, R. Ahmadian, R. Falconer, Tidal range energy resource and optimization – past perspectives and future challenges, Renew. Energy 127 (2018) 763–778, http://dx.doi.org/10.1016/j.renene.2018.05.007.

[14] K. Gunn, C. Stock-Williams, Quantifying the global wave power resource, Renew. Energy 44 (2012-08) 296–304, http://dx.doi.org/10.1016/j.renene.2012.01.101.

[15] F. Taveira-Pinto, G. Iglesias, P. Rosa-Santos, Z.D. Deng, Preface to special topic: Marine renewable energy, J. Renew. Sustain. Energy 7 (6) (2015) 61601, http://dx.doi.org/10.1063/1.4939086.

[16] UNTC, Paris agreement, 2023, URL https://treaties.un.org/pages/ViewDetails.aspx?src=TREATY&mtdsg_no=XXVII-7-d&chapter=27&clang=_en. Online; (Accessed 31 August 2023).

[17] Supergen, Wave Energy Road Map, Eng. Phys. Sci. Res. Counc. (2020) 5–5, URL https://supergen-ore.net/uploads/resources/Wave_Energy_Road_Map_-_Realising_the_potential_of_Wave_Energy_in_the_next_10_to_15_years.pdf.
[18] S. Astariz, G. Iglesias, The economics of wave energy: A review, Renew. Sustain. Energy Rev. 45 (2015) 397–408, http://dx.doi.org/10.1016/j.rser.2015.01.061.
[19] EERE, Exploring Opportunities for Marine Renewable Energy in Maritime Markets, (April) U.S.Department of Energy, 2019, p. 170, URL https://www.ocean-energy-systems.org/about-oes/what-is-ocean-energy/.
[20] Q. Gao, S.S. Khan, N. Sergiienko, N. Ertugrul, M. Hemer, M. Negnevitsky, B. Ding, Assessment of wind and wave power characteristic and potential for hybrid exploration in Australia, Renew. Sustain. Energy Rev. 168 (2022) 112747, http://dx.doi.org/10.1016/j.rser.2022.112747.
[21] Y. Wen, B. Kamranzad, P. Lin, Joint exploitation potential of offshore wind and wave energy along the south and southeast coasts of China, Energy 249 (2022) 123710, http://dx.doi.org/10.1016/j.energy.2022.123710.
[22] D. Christie, S.P. Neill, P. Arnold, Characterising the wave energy resource of lanzarote, canary islands, Renew. Energy 206 (2023) 1198–1211, http://dx.doi.org/10.1016/j.renene.2023.02.126.
[23] S.P. Neill, Wave resource characterization and co-location with offshore wind in the irish sea, Renew. Energy 222 (2024) 119902.
[24] E.D. Stoutenburg, N. Jenkins, M.Z. Jacobson, Power output variations of co-located offshore wind turbines and wave energy converters in california, Renew. Energy 35 (12) (2010) 2781–2791, http://dx.doi.org/10.1016/j.renene.2010.04.033, URL https://www.sciencedirect.com/science/article/pii/S0960148110002004.
[25] F. Fusco, G. Nolan, V.J. Ringwood, Variability reduction through optimal combination of wind/wave resources – an irish case study, Energy 35 (1) (2010) 314–325, http://dx.doi.org/10.1016/j.energy.2009.09.023.
[26] L. Castro-Santos, E. Martins, C. Guedes Soares, Economic comparison of technological alternatives to harness offshore wind and wave energies, Energy 140 (2017) 1121–1130, http://dx.doi.org/10.1016/j.energy.2017.08.103, URL https://www.sciencedirect.com/science/article/pii/S0360544217314792.
[27] H. Yazdi, H.R. Ghafari, H. Ghassemi, G. He, M. Karimirad, Wave power extraction by Multi-Salter's duck WECs arrayed on the floating offshore wind turbine platform, Energy 278 (2023) 127930, http://dx.doi.org/10.1016/j.energy.2023.127930, URL https://www.sciencedirect.com/science/article/pii/S0360544223013245.
[28] J. Kluger, M. Haji, A. Slocum, The power balancing benefits of wave energy converters in offshore wind-wave farms with energy storage, Appl. Energy 331 (2023) 120389, http://dx.doi.org/10.1016/j.apenergy.2022.120389.
[29] S. Astariz, C. Perez-Collazo, J. Abanades, G. Iglesias, Co-located wind-wave farm synergies (operation & maintenance): A case study, Energy Convers. Manage. 91 (2015) 63–75, http://dx.doi.org/10.1016/j.enconman.2014.11.060.
[30] [dataset] ECMWF, ERA5 monthly averaged data on single levels from 1940 to present, 2023, URL https://cds.climate.copernicus.eu/cdsapp#!/dataset/reanalysis-era5-single-levels-monthly-means?tab=form. Online; (Accessed 02 May 2023).
[31] H. Hersbach, B. Bell, P. Berrisford, S. Hirahara, A. Horányi, J. Muñoz-Sabater, J. Nicolas, C. Peubey, R. Radu, D. Schepers, A. Simmons, C. Soci, S. Abdalla, X. Abellan, G. Balsamo, P. Bechtold, G. Biavati, J. Bidlot, M. Bonavita, G. De Chiara, P. Dahlgren, D. Dee, M. Diamantakis, R. Dragani, J. Flemming, R. Forbes, M. Fuentes, A. Geer, L. Haimberger, S. Healy, R.J. Hogan, E. Hólm, M. Janisková, S. Keeley, P. Laloyaux, P. Lopez, C. Lupu, G. Radnoti, P. de Rosnay, I. Rozum, F. Vamborg, S. Villaume, J.N. Thépaut, The ERA5 global reanalysis, Q. J. R. Meteorol. Soc. 146 (730) (2020-07-01) 1999–2049, http://dx.doi.org/10.1002/QJ.3803.
[32] J.P. Murcia, M.J. Koivisto, G. Luzia, B.T. Olsen, A.N. Hahmann, P.E. Sørensen, M. Als, Validation of European-scale simulated wind speed and wind generation time series, Appl. Energy 305 (2022) 117794, http://dx.doi.org/10.1016/j.apenergy.2021.117794.
[33] J. Liu, B. Li, W. Chen, J. Li, J. Yan, Evaluation of ERA5 wave parameters with in situ data in the south China sea, Atmosphere 13 (6) (2022) http://dx.doi.org/10.3390/atmos13060935.
[34] ECMWF, IFS documentation CY47R3 – part VII: ECMWF wave model, IFS Documentation, IFS Doc. CY47R3 (2021) http://dx.doi.org/10.21957/zz4bj65vr.
[35] S.A. Hsu, E.A. Meindl, D.B. Gilhousen, Determining the power-law wind-profile exponent under near-neutral stability conditions at sea, J. Appl. Meteorol. Clim. 33 (6) (1994) 757–765.
[36] Q. Vu Dinh, Q.-V. Doan, T. Ngo-Duc, V. Nguyen Dinh, N. Dinh Duc, Offshore wind resource in the context of global climate change over a tropical area, Appl. Energy 308 (2022) 118369, http://dx.doi.org/10.1016/j.apenergy.2021.118369, URL https://www.sciencedirect.com/science/article/pii/S0306261921016123.
[37] C. Kalogeri, G. Galanis, C. Spyrou, D. Diamantis, F. Baladima, M. Koukoula, G. Kallos, Assessing the European offshore wind and wave energy resource for combined exploitation, Renew. Energy 101 (2017) 244–264, http://dx.doi.org/10.1016/j.renene.2016.08.010.
[38] P. Bortolotti, H.C. Tarres, K.L. Dykes, K. Merz, L. Sethuraman, D. Verelst, F. Zahle, Systems engineering in wind energy – WP2.1 reference wind turbines, Natl. Renew. Energy Lab. (May) (2019).
[39] E. Gaertner, J. Rinker, L. Sethuraman, B. Anderson, F. Zahle, G. Barter, IEA Wind TCP Task 37: Definition of the IEA 15 MW Offshore Reference Wind Turbine, Technical Report NREL/TP-5000-75698 March 2020, 2020, pp. 1–44.
[40] G. Lavidas, Selection index for wave energy deployments (SIWED): A near-deterministic index for wave energy converters, Energy 196 (2020) 117131, http://dx.doi.org/10.1016/j.energy.2020.117131, URL https://www.sciencedirect.com/science/article/pii/S0360544220302383.
[41] 4Coffshore, Global offshore wind farm database, 2023, URL https://www.4coffshore.com/windfarms. Online; (Accessed 17 April 2023).
[42] A.G. Majidi, B. Bingölbali, A. Akpınar, E. Rusu, Wave power performance of wave energy converters at high-energy areas of a semi-enclosed sea, Energy 220 (2021) 119705, http://dx.doi.org/10.1016/j.energy.2020.119705.
[43] S. Bozzi, G. Besio, G. Passoni, Wave power technologies for the mediterranean offshore: Scaling and performance analysis, Coast. Eng. 136 (2018) 130–146, http://dx.doi.org/10.1016/j.coastaleng.2018.03.001.
[44] S. Astariz, G. Iglesias, Accessibility for operation and maintenance tasks in co-located wind and wave energy farms with non-uniformly distributed arrays, Energy Convers. Manage. 106 (2015) 1219–1229.
[45] SeaPower, Harnessing wave energy, 2023, URL https://www.seapower.ie/. Online; (Accessed 20 August 2023).
[46] G. Sinden, Variability of UK marine resources, The Carbon Trust, London, 2005.
[47] N. Tapper, L. Hurry, Australia's Weather Patterns: an Introductory Guide, Dellasta, 1993.
[48] S. Rafiq, C. Pattiaratchi, I. Janeković, Dynamics of the land–sea breeze system and the surface current response in South-West Australia, J. Mar. Sci. Eng. 8 (11) (2020) http://dx.doi.org/10.3390/jmse8110931.
[49] R.A. Gideon, E. Bou-Zeid, Collocating offshore wind and wave generators to reduce power output variability: A multi-site analysis, Renew. Energy 163 (2021) 1548–1559, http://dx.doi.org/10.1016/j.renene.2020.09.047.
[50] W. Musial, P. Spitsen, P. Duffy, P. Beiter, M. Shields, D.M. Hernando, R. Hammond, M. Marquis, J. King, S. Sriharan, Offshore Wind Market Report: 2023 Edition, Tech. Rep., 2023.
[51] M. Veigas, M. López, P. Romillo, R. Carballo, A. Castro, G. Iglesias, A proposed wave farm on the galician coast, Energy Convers. Manage. 99 (2015) 102–111, http://dx.doi.org/10.1016/j.enconman.2015.04.033.